

## 1 Supplementary information

2 **Title:** A green synthesis of PEI@nano-SiO<sub>2</sub> adsorbent from coal fly ash: Selective and efficient CO<sub>2</sub>  
3 adsorption from biogas

4 Xuehua Shen,<sup>a,b</sup> Feng Yan,<sup>a,c,\*</sup> Chunyan Li,<sup>a</sup> Zhen Zhang,<sup>a,b</sup> Zuotai Zhang<sup>a,c,\*</sup>

5 <sup>a</sup> School of Environmental Science and Engineering, Guangdong Provincial Key Laboratory of Soil and  
6 Groundwater Pollution Control, Southern University of Science and Technology, Shenzhen 518055, P.R. China

7 <sup>b</sup> School of Environment, Harbin Institute of Technology, Harbin 150090, P.R. China.

8 <sup>c</sup> Key Laboratory of Municipal Solid Waste Recycling Technology and Management of Shenzhen City, Shenzhen  
9 518055, P.R. China.

### 10 \* Corresponding author:

11 Prof. Zuotai Zhang, E-mail address: [zhangzt@sustech.edu.cn](mailto:zhangzt@sustech.edu.cn)

12 Dr. Feng Yan, E-mail address: [yanf@sustech.edu.cn](mailto:yanf@sustech.edu.cn)

13 This supporting information includes:

### 14 1. Experimental:

15 1.1 Synthesis of nano-SiO<sub>2</sub> supports from coal fly ash

16 1.2 Calculation of silanol content and -OH density

### 17 2. Results:

18 **Table S1.** Chemical composition of coal fly ash.

19 **Table S2.** Structural properties of the synthetic PEI@nano-SiO<sub>2</sub> adsorbents with different PEI loadings (supported  
20 by “SiO<sub>2</sub>-6%”).

21 **Figure S1.** SEM images of the nano-SiO<sub>2</sub> supports synthesized from different Na<sub>2</sub>SiO<sub>3</sub> concentrations of 20–80  
22 g·L<sup>-1</sup>.

23 **Figure S2.** (a) FT-IR spectra and (b) TG curves of nano-SiO<sub>2</sub> supports synthesized from different Na<sub>2</sub>SiO<sub>3</sub>  
24 concentrations of 20–80 g·L<sup>-1</sup>.

25 **Figure S3.** (a) N<sub>2</sub> adsorption/desorption isotherms and (b) pore size distributions of PEI@nano-SiO<sub>2</sub> adsorbents  
26 with different nano-SiO<sub>2</sub> supports (40% PEI loading).

27 **Figure S4.** (a) N<sub>2</sub> adsorption/desorption isotherms and (b) pore size distributions of PEI@nano-SiO<sub>2</sub> adsorbents  
28 with different PEI loadings (supported by “SiO<sub>2</sub>-6%”).

29 **Figure S5.** (a) TG and (b) DTG curves of the synthetic PEI@nano-SiO<sub>2</sub> adsorbents with different PEI loadings  
30 (supported by “SiO<sub>2</sub>-6%”).

31 **Figure S6.** SEM images of the synthetic PEI@nano-SiO<sub>2</sub> adsorbents with different PEI loadings (supported by  
32 “SiO<sub>2</sub>-6%”).

33 **Figure S7.** (a) The thermal stability curves and (b) adsorption curves of the “40%-PEI@SiO<sub>2</sub>-6%” adsorbent and  
34 the “40%-PEI@Commercial SiO<sub>2</sub>”; (c) and (d) the breakthrough curves of CO<sub>2</sub>/CH<sub>4</sub> adsorption using the “40%-  
35 PEI@SiO<sub>2</sub>-6%” adsorbent and the “40%-PEI@Commercial SiO<sub>2</sub>” (adsorption at 90 °C; total flow rate: 30 mL/min;  
36 inlet CO<sub>2</sub> concentration: 40 vol. %).

37 **Figure S8.** FT-IR spectra of fresh PEI@nano-SiO<sub>2</sub> adsorbents (a) with different nano-SiO<sub>2</sub> supports (40% PEI  
38 loading), and (b) with different PEI loadings (supported by “SiO<sub>2</sub>-6%”).

39 **Figure S9.** (a) FT-IR spectra of the regenerated “40%-PEI@SiO<sub>2</sub>-6%” in pure CO<sub>2</sub> atmosphere at different  
40 temperature of 120–165 °C; (b) cyclic performance of “40%-PEI@SiO<sub>2</sub>-6%” regenerated under pure CO<sub>2</sub>  
41 atmosphere for 15 min at different temperatures of 135–165 °C (adsorption at 90 °C for 30 min).

42 **Figure S10.** FT-IR spectra of the regenerated PEI@nano-SiO<sub>2</sub> adsorbents after 50 cycles (a) under pure Ar  
43 atmosphere at 120 °C for 15 min; (b) under pure CO<sub>2</sub> atmosphere at 150 °C for 15 min (adsorption at 90 °C for 30  
44 min). (c) cyclic performance of “40%-PEI@SiO<sub>2</sub>-6%” and “40%-PEI@Commercial SiO<sub>2</sub>” regenerated under pure  
45 CO<sub>2</sub> atmosphere for 15 min at 150 °C (adsorption at 90 °C for 30 min).

## 46 1.1 Synthesis of nano-SiO<sub>2</sub> supports from coal fly ash

47 Preheated and sieved 10 g CFA and 5 g NaOH were mixed with 15 mL of ultrapure water in a  
48 100mL sealed Teflon-lined reactor (BeiLun, China) and then the mixture reacted at 110 °C for 0.5 h  
49 with stirring (300 rpm). Immediately after the experiment, the reacted suspension was filtered several  
50 times with ultrapure water to obtain the leaching solution (Na<sub>2</sub>SiO<sub>3</sub> solution). A certain quantity of  
51 leaching solution was placed in the Teflon-lined reactor, and the concentration of Na<sub>2</sub>SiO<sub>3</sub> (C<sub>Na<sub>2</sub>SiO<sub>3</sub></sub>,  
52 g·L<sup>-1</sup>) in the mixture was diluted to 80, 70, 60, 50, 40, 30 and 20 g·L<sup>-1</sup> by adding ultrapure water,  
53 respectively. A constant flow of 40 mL·min<sup>-1</sup> (15 vol % CO<sub>2</sub> and 85 vol % N<sub>2</sub>) was injected to purify  
54 the mixture and assist the silica precipitation. The purification process was conducted at 80 °C with

55 stirring (300 rpm) until the pH value decreased to 10.8-11.3 (~15 min); the purified mixture was then  
 56 obtained through filtration. Subsequently, the precipitation process was conducted using the purified  
 57 mixture under the same conditions for another 3-7 h. Finally, the precipitation was filtered, washed  
 58 and dried at 105 °C for 12 h under vacuum (<1 mmHg) to obtain nano-SiO<sub>2</sub> supports.

## 59 1.2 Calculation of silanol content and -OH density

60 **Figure S2(b)** showed the thermogravimetric analysis of nano-SiO<sub>2</sub> in the range of 50–800 °C. The  
 61 weight loss of adsorbents could be divided into three stages: 50–200 °C, 200–600 °C and 600–800  
 62 °C, respectively [1], and the weight loss of each stage was shown in Table 2. Accordingly, the weight  
 63 loss on the first stage (below 200 °C) was caused by the release of physical and chemical adsorbed  
 64 water on nano silica surface [2]. On the second stage (200–600 °C), the weight loss was mainly  
 65 attributed to dehydroxylation following the condensation of germinal silanol and vicinal silanol. And  
 66 the weight loss in the last stage (above 600 °C) was mainly due to the loss of isolated silanol [3].  
 67 Depending on the weight loss, the silanol content ( $N_{OH}$ ) and the silanol density ( $C_{OH}$ ) of different  
 68 nano-SiO<sub>2</sub> supports can be confirmed with formulas (1) and (2), respectively [4].

$$69 \quad N_{OH} = \frac{2 \times (W_{200} - W_{800})}{M_{H_2O}} \times 1000 \quad (1)$$

$$70 \quad C_{OH} = \frac{2 \times (W_{200} - W_{800})}{M_{H_2O}} \times \frac{N_A}{S_{BET} \times 10^{18}} \quad (2)$$

71 Where  $W_{200}$  and  $W_{800}$  are the weight of nano-SiO<sub>2</sub> samples at the temperature of 200 and 800 °C,  
 72 respectively;  $M_{H_2O}$  is the molecular weight of water;  $N_A$  is the Avogadro constant;  $S_{BET}$  is the specific  
 73 surface area of nano-SiO<sub>2</sub> samples.

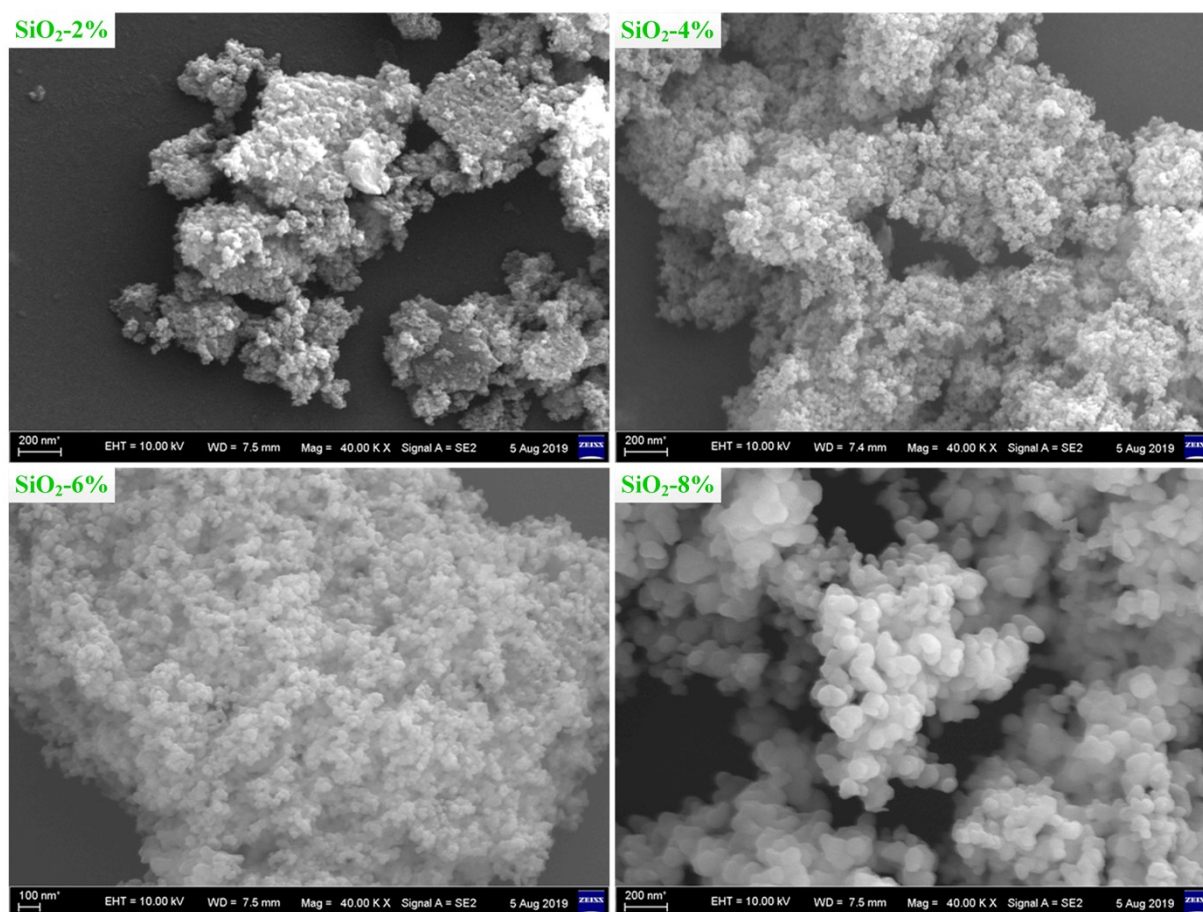
74 **Table S1** Chemical composition of coal fly ash.

Samples	SiO <sub>2</sub> (wt. %)	Al <sub>2</sub> O <sub>3</sub> (wt. %)	Fe <sub>2</sub> O <sub>3</sub> (wt. %)	Na <sub>2</sub> O (wt. %)	CaO (wt. %)	TiO <sub>2</sub> (wt. %)	MgO (wt. %)	K <sub>2</sub> O (wt. %)	Others (wt. %)
CFA	52.00	36.51	5.03	0.14	2.61	1.80	0.33	0.77	0.81

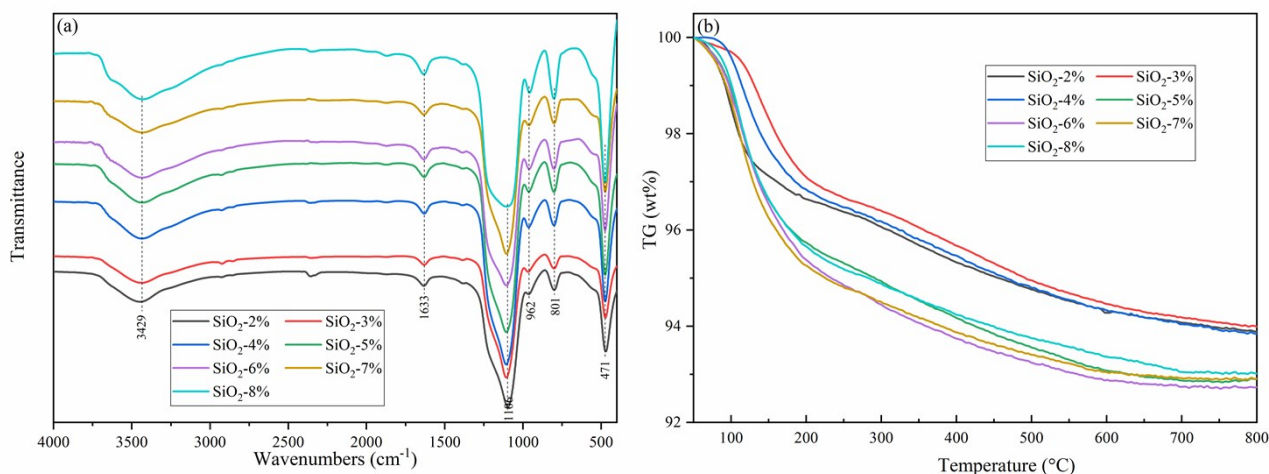
76 **Table S2** Structural properties of the synthetic PEI@nano-SiO<sub>2</sub> adsorbents with different PEI loadings (supported  
 77 by “SiO<sub>2</sub>-6%”).

Samples	$S_{\text{BET}}^a$ (m <sup>2</sup> ·g <sup>-1</sup> )	$V_{\text{pore}}^b$ (cm <sup>3</sup> ·g <sup>-1</sup> )	$D_{\text{BJH}}^c$ (nm)
10%-PEI@SiO <sub>2</sub> -6%	47.0	0.47	36.74
20%-PEI@SiO <sub>2</sub> -6%	30.6	0.39	47.50
30%-PEI@SiO <sub>2</sub> -6%	17.2	0.16	34.00
35%-PEI@SiO <sub>2</sub> -6%	8.99	0.062	25.74
40%-PEI@SiO <sub>2</sub> -6%	7.7	0.034	16.46
45%-PEI@SiO <sub>2</sub> -6%	3.35	0.018	20.08

78 <sup>a</sup>  $S_{\text{BET}}$ , specific surface area; <sup>b</sup>  $V_{\text{pore}}$ , total pore volume; <sup>c</sup>  $D_{\text{BJH}}$ , average pore size.

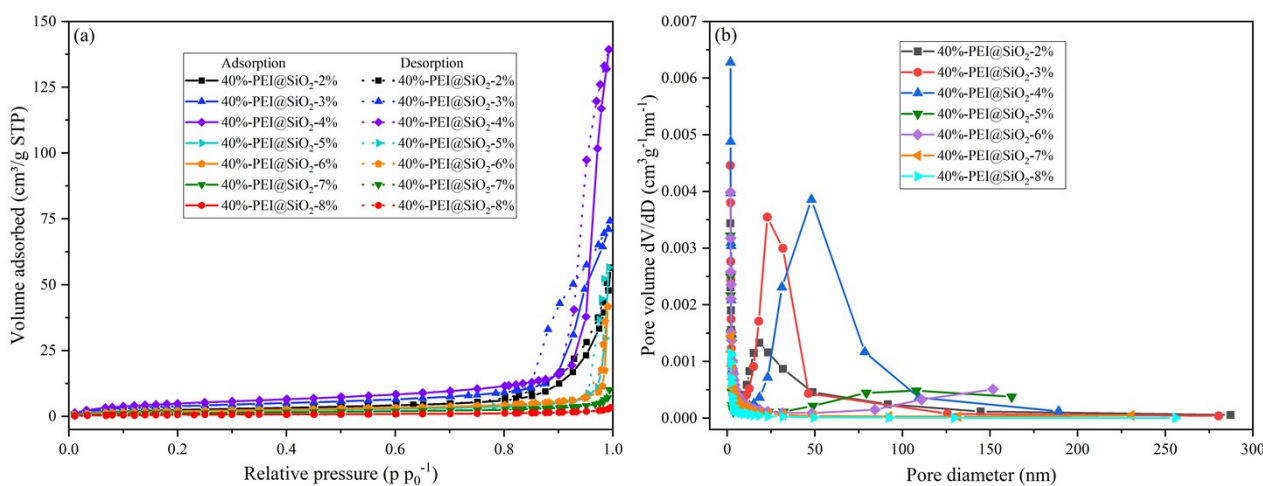


79  
 80 **Figure S1.** SEM images of the nano-SiO<sub>2</sub> supports synthesized from different Na<sub>2</sub>SiO<sub>3</sub> concentrations of 20–80  
 81 g·L<sup>-1</sup>.



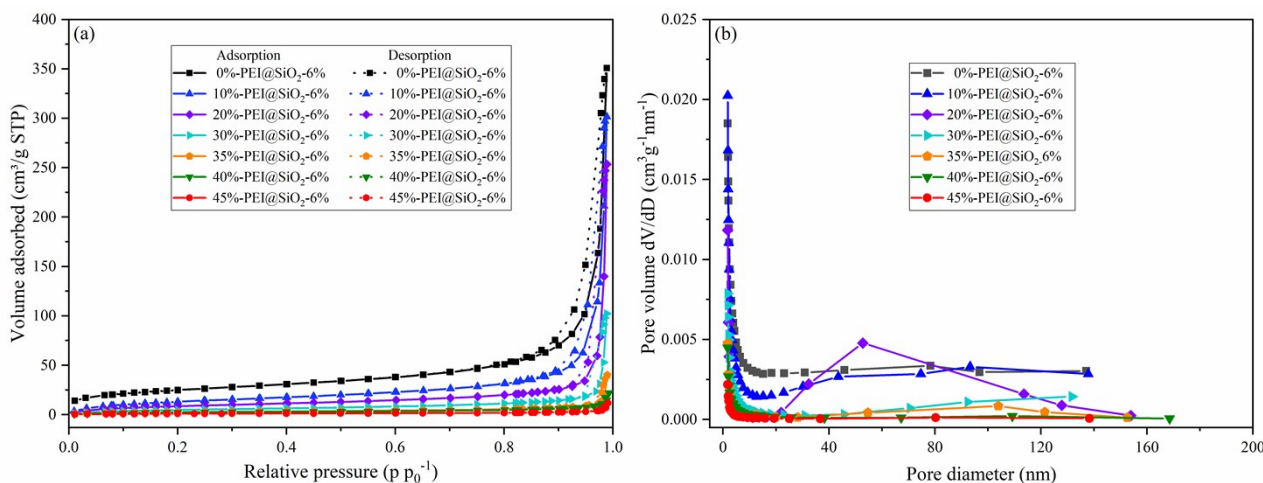
82

83 **Figure S2.** (a) FT-IR spectra and (b) TG curves of nano-SiO<sub>2</sub> supports synthesized from different Na<sub>2</sub>SiO<sub>3</sub>  
 84 concentrations of 20–80 g·L<sup>-1</sup>.



85

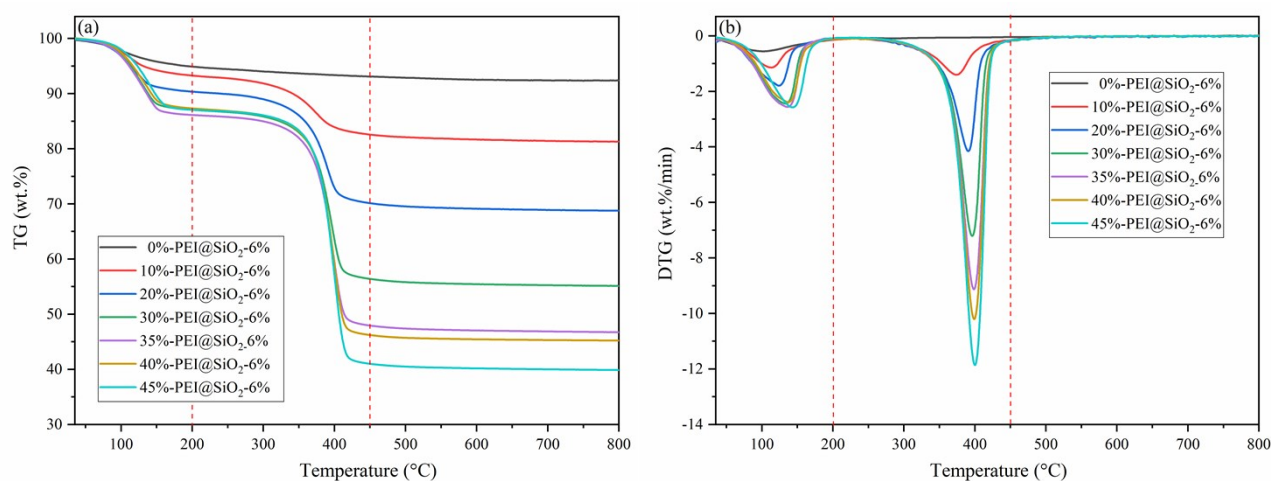
86 **Figure S3.** (a) N<sub>2</sub> adsorption/desorption isotherms and (b) pore size distributions of PEI@nano-SiO<sub>2</sub> adsorbents  
 87 with different nano-SiO<sub>2</sub> supports (40% PEI loading).



88

89 **Figure S4.** (a) N<sub>2</sub> adsorption/desorption isotherms and (b) pore size distributions of PEI@nano-SiO<sub>2</sub> adsorbents

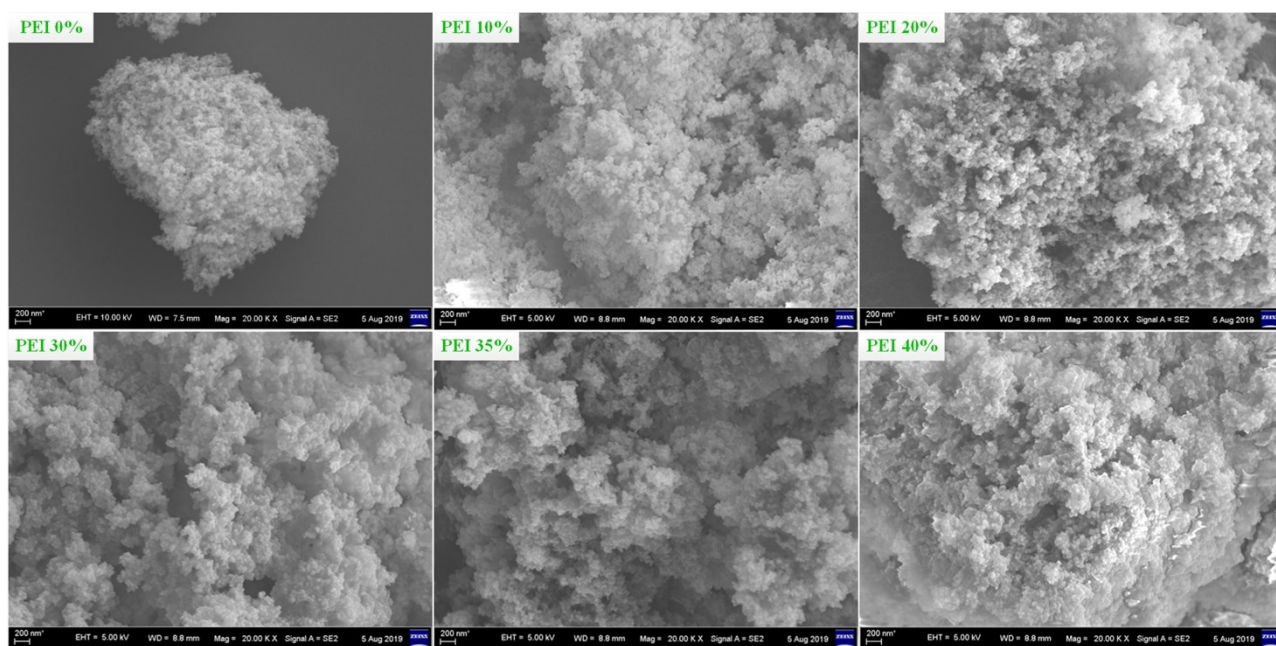
90 with different PEI loadings (supported by “SiO<sub>2</sub>-6%”).



91

92 **Figure S5.** (a) TG and (b) DTG curves of the synthetic PEI@nano-SiO<sub>2</sub> adsorbents with different PEI loadings

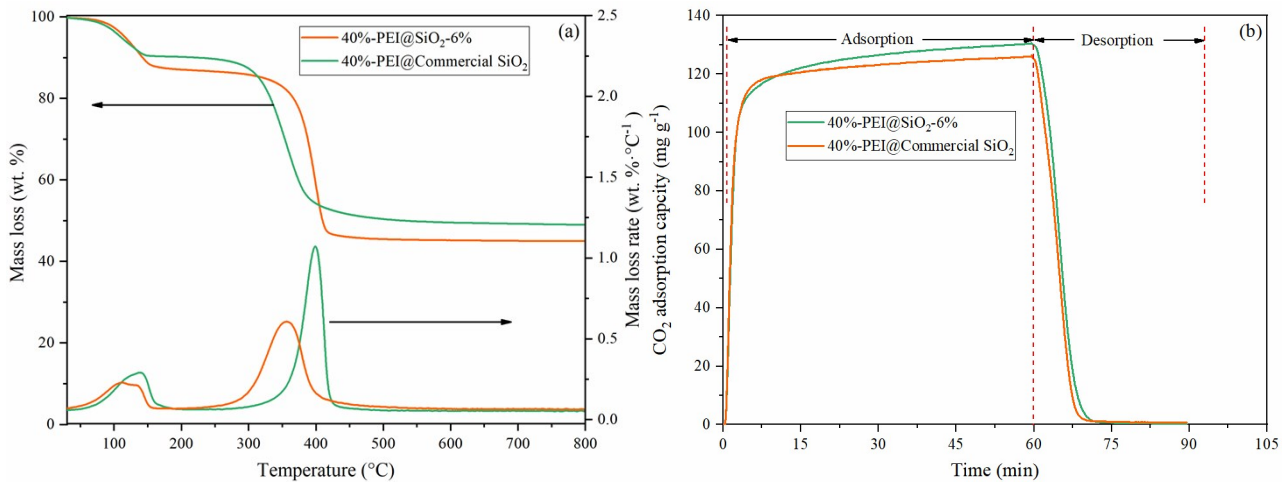
93 (supported by “SiO<sub>2</sub>-6%”).



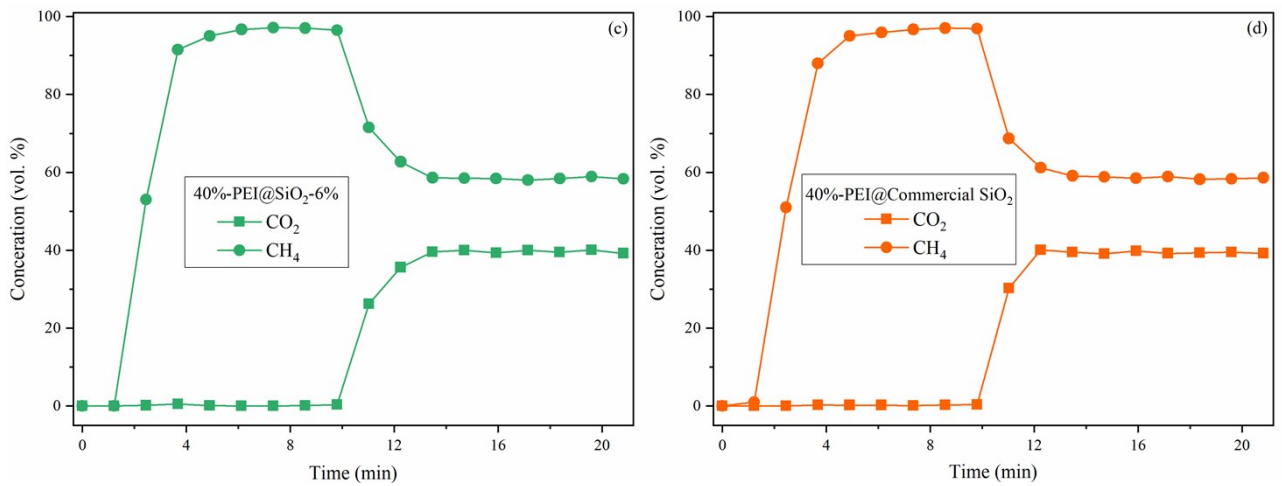
94

95 **Figure S6.** SEM images of the synthetic PEI@nano-SiO<sub>2</sub> adsorbents with different PEI loadings (supported by

96 “SiO<sub>2</sub>-6%”).

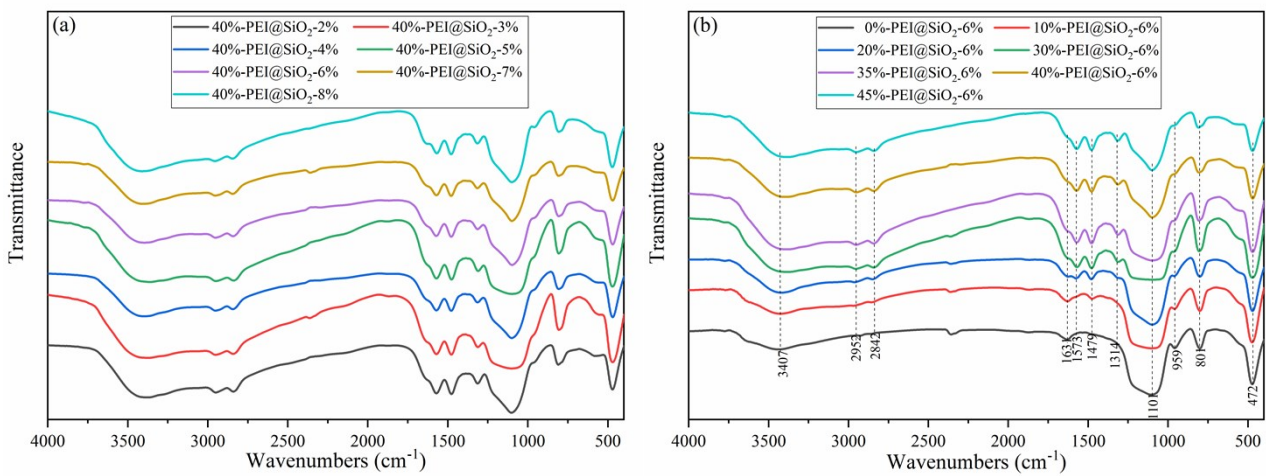


97



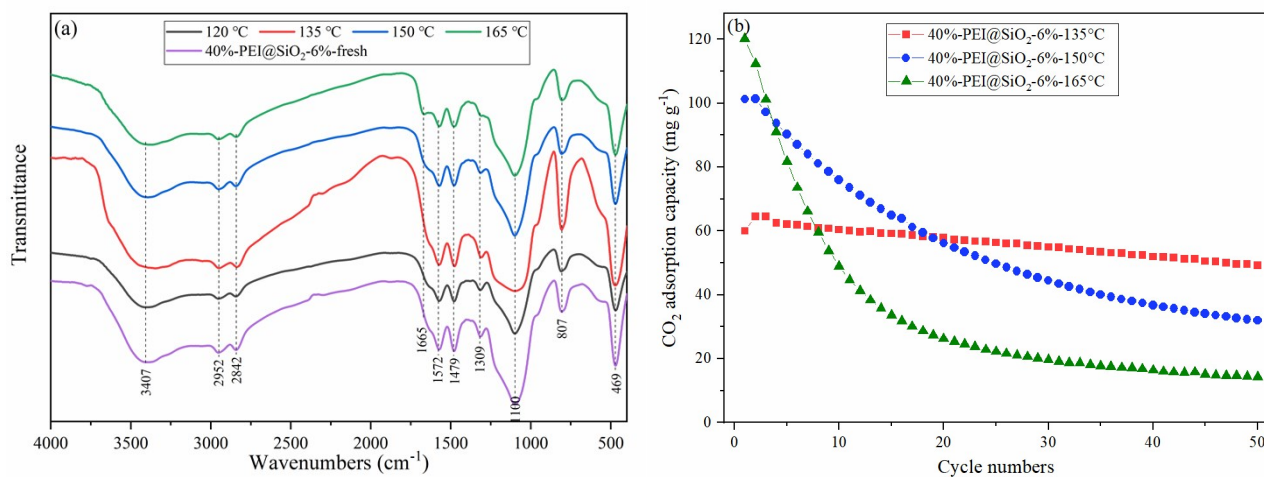
98

99 **Figure S7.** (a) The thermal stability curves and (b) adsorption curves of the “40%-PEI@SiO<sub>2</sub>-6%” adsorbent and  
 100 the “40%-PEI@Commercial SiO<sub>2</sub>”; (c) and (d) the breakthrough curves of CO<sub>2</sub>/CH<sub>4</sub> adsorption using the “40%-  
 101 PEI@SiO<sub>2</sub>-6%” adsorbent and the “40%-PEI@Commercial SiO<sub>2</sub>” (adsorption at 90 °C; total flow rate: 30 mL/min;  
 102 inlet CO<sub>2</sub> concentration: 40 vol. %).



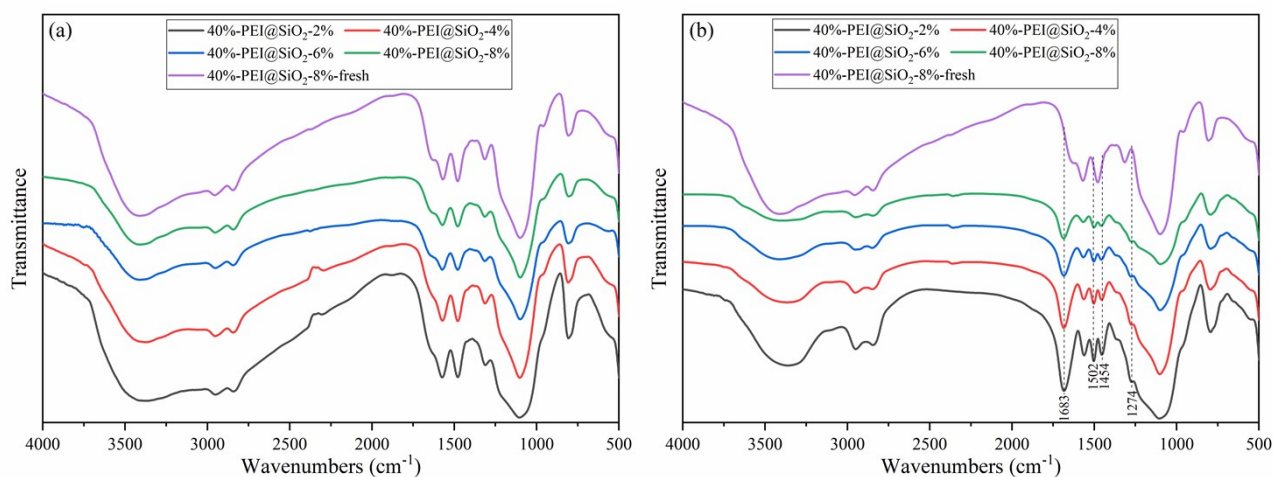
103

104 **Figure S8.** FT-IR spectra of fresh PEI@nano-SiO<sub>2</sub> adsorbents (a) with different nano-SiO<sub>2</sub> supports (40% PEI  
 105 loading), and (b) with different PEI loadings (supported by “SiO<sub>2</sub>-6%”).



106

107 **Figure S9.** (a) FT-IR spectra of the regenerated “40%-PEI@SiO<sub>2</sub>-6%” in pure CO<sub>2</sub> atmosphere at different  
 108 temperature of 120–165 °C; (b) cyclic performance of “40%-PEI@SiO<sub>2</sub>-6%” regenerated under pure CO<sub>2</sub>  
 109 atmosphere for 15 min at different temperatures of 135–165 °C (adsorption at 90 °C for 30 min).



110

111

112 **Figure S10.** FT-IR spectra of the regenerated PEI@nano-SiO<sub>2</sub> adsorbents after 50 cycles (a) under pure Ar  
 113 atmosphere at 120 °C for 15 min; (b) under pure CO<sub>2</sub> atmosphere at 150 °C for 15 min (adsorption at 90 °C for 30  
 114 min); (c) cyclic performance of “40%-PEI@SiO<sub>2</sub>-6%” and “40%-PEI@Commercial SiO<sub>2</sub>” regenerated under pure



115 CO<sub>2</sub> atmosphere for 15 min at 150 °C (adsorption at 90 °C for 30 min).

## 116 **References**

117 [1] Li K-M, Jiang J-G, Tian S-C, Chen X-J, Yan F. Influence of silica types on synthesis and performance of amine–  
118 silica hybrid materials used for CO<sub>2</sub> capture. *J Phys Chem C* 2014;118(5):2454-62.

119 [2] Wang L, Yang RT. Increasing selective CO<sub>2</sub> adsorption on amine-grafted SBA-15 by increasing silanol  
120 density. *J Phys Chem C* 2011;115(43):21264-72.

121 [3] Cerveny S, Schwartz GA, Otegui J, Colmenero J, Loichen J, Westermann S. Dielectric study of hydration  
122 water in silica nanoparticles. *J Phys Chem C* 2012;116(45):24340-9.

123 [4] Ek S, Root A, Peussa M, Niinistö L. Determination of the hydroxyl group content in silica by thermogravimetry  
124 and a comparison with <sup>1</sup>H MAS NMR results. *Thermochim Acta* 2001;379(1):201-12.